

Cite this: *Soft Matter*, 2014, 10, 7468

# Digital colloids: reconfigurable clusters as high information density elements†

Carolyn L. Phillips,<sup>ab</sup> Eric Jankowski,<sup>cd</sup> Bhaskar Jyoti Krishnatreya,<sup>e</sup>  
Kazem V. Edmond,<sup>f</sup> Stefano Sacanna,<sup>g</sup> David G. Grier,<sup>h</sup> David J. Pine<sup>i</sup>  
and Sharon C. Glotzer<sup>\*j</sup>

Through the design and manipulation of discrete, nanoscale systems capable of encoding massive amounts of information, the basic components of computation are open to reinvention. These components will enable tagging, memory storage, and sensing in unusual environments – elementary functions crucial for soft robotics and “wet computing”. Here we show how reconfigurable clusters made of  $N$  colloidal particles bound flexibly to a central colloidal sphere have the capacity to store an amount of information that increases as  $O(N \ln(N))$ . Using Brownian dynamics simulations, we predict dynamical regimes that allow for information to be written, saved, and erased. We experimentally assemble an  $N = 4$  reconfigurable cluster from chemically synthesized colloidal building blocks, and monitor its equilibrium dynamics. We observe state switching in agreement with simulations. This cluster can store one bit of information, and represents the simplest digital colloid.

Received 12th April 2014

Accepted 19th June 2014

DOI: 10.1039/c4sm00796d

www.rsc.org/softmatter

The desire for pervasive embedded computing across scales and environments demands we consider alternative ways to store and manipulate data other than transistors. Alternative approaches to traditional computation include computing with DNA,<sup>1–5</sup> Belousov–Zhabotinsky chemical reactions,<sup>6</sup> microfluidic bubble circuits<sup>7</sup> and chemosensors.<sup>8</sup> Of these alternative approaches to computation, DNA computing has received the most attention and has advanced the furthest. The storage capabilities of DNA were recently highlighted with the writing and subsequent reading of a 5.25 megabit book on DNA.<sup>9</sup> Ref. 5

further shows DNA's potential for biological *in situ* universal computing. The use of DNA and other off-chip computing elements is driven by new technologies including autonomous “softbots”<sup>10</sup> and 3D printed high-functioning materials,<sup>11–13</sup> which require information storage, switchable memory elements, and parallel computation. Microscopic colloidal particles are another promising alternative computing architecture, as thermodynamically large ensembles of these particles can perform astronomical numbers of calculations simultaneously.<sup>14</sup> Such colloidal computational elements could be dispersed throughout a medium to perform *in situ* calculations based on the locally available data, or to store information in an easily transported fluid medium.

The objective of using new, soft matter, digital nanostructures should not be to simply emulate digital processes *in silico*. Alternative computing paradigms designed for massively parallel and distributed systems include amorphous computing<sup>15</sup> – a new branch of computational science that studies how coherent functional behavior can be achieved from distributed, asynchronous, locally interacting, computing elements. Servat and Drogoul<sup>16</sup> propose that a new powerful form of computing could be realized by constructing an amorphous computing medium from a population of lightweight computing elements that respond to changes in their environment through self-organization. We propose that a system of reconfigurable colloidal particles is a natural candidate for such a system.

Recent advances in colloidal synthesis<sup>17,18</sup> have created a vast design space of particles with precisely engineered sizes and shapes whose interactions with other particles are both

<sup>a</sup>Applied Physics Program, University of Michigan, Ann Arbor, Michigan, 48109, USA<sup>b</sup>Mathematics and Computer Science Division, Argonne National Laboratory, Argonne, Illinois, 60439, USA<sup>c</sup>Department of Chemical Engineering, University of Michigan, Ann Arbor, Michigan, 48109, USA<sup>d</sup>Department of Chemical Engineering, University of Colorado, Boulder, Colorado, 80309, USA<sup>e</sup>Department of Physics and Center for Soft Matter Research, New York University, New York, New York, 10003, USA<sup>f</sup>Department of Physics and Center for Soft Matter Research, New York University, New York, New York, 10003, USA<sup>g</sup>Department of Chemistry, New York University, New York, New York, 10003, USA<sup>h</sup>Department of Physics and Center for Soft Matter Research, New York University, New York, New York, 10003, USA<sup>i</sup>Department of Physics and Center for Soft Matter Research, New York University, New York, New York, 10003, USA<sup>j</sup>Department of Chemical Engineering, Department of Materials Science and Engineering, Applied Physics Program, University of Michigan, Ann Arbor, Michigan, 48109, USA. E-mail: sglotzer@umich.edu

† Electronic supplementary information (ESI) available. See DOI: 10.1039/c4sm00796d

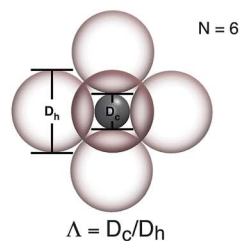
directional and specific. Dispersions of such colloidal particles constitute a new paradigm of soft programmable matter.<sup>19</sup> Two recent examples of particular relevance to the present work are dimpled colloidal spheres with shape-specific interactions,<sup>20,21</sup> which can be assembled into reconfigurable clusters. Information stored in colloidal materials can be retrieved in a variety of ways, from direct observation *via* optical microscopy to inference based on macroscopic properties. Here, we describe the first steps in combining these features to create high-density computing elements that we dub *digital colloids*.

Digital colloids are defined by three essential characteristics. First, each colloidal cluster must be able to switch among distinguishable microstates, referred to below as simply “states”, each with known probability of occurrence. The set of all such accessible states determines the amount of information that a cluster can store. A cluster with two unique states, for example, can store one bit, while a cluster with 256 unique states can store a byte. For the digital colloids we describe here, each cluster state corresponds to the same cluster morphology, but is distinguishable only insofar as the particles themselves are distinguishable. Second, it must be possible to disable or enable the clusters’ ability to switch. *Locking* a cluster’s configuration preserves its information for readout. *Unlocking* enables the cluster to perform computations. Third, a method must be available to set a cluster’s state deterministically under external control, thereby allowing information to be stored and algorithms to be programmed. After describing a class of colloidal clusters that have these characteristics, we present a working experimental realization of a two-state, switchable, digital colloidal element capable of storing a single bit of information. We conclude by proposing several examples of how digital colloids can be used in practical applications. Just as ref. 1 changed the way we think about performing computation by introducing the idea of “soft computation”, we anticipate that reconfigurable colloidal clusters like those we propose here may be used as “context-aware” distributed information storage devices, permitting novel ways to perform sensing and computing in solvent-based chemical processes and biological systems, and may even provide ways to interface traditional computers with computations being performed in the bloodstream or brain.

As design and control of colloidal scale matter increase, one can envision many creative ways that systems with switchable

morphologies could be employed to store information. Our design for digital colloids is motivated by the *spherical code* problem. A long-studied mathematical problem, the  $N$ th spherical code (SC) solution<sup>22–24</sup> gives the densest packing of  $N$  hard spheres of diameter  $d$  in contact with a central sphere of unit diameter. The diameter ratio  $\Lambda$  of the central sphere to the outer spheres, illustrated in Fig. 1, characterizes the cluster. The densest packing for any  $N$  is achieved for a diameter ratio  $\Lambda_{SC} = 1/d_{SC}$ . Values of  $\Lambda_{SC}$  are tabulated for up to  $N = 130$  in ref. 25. A cluster of  $N$  spheres in its spherical code structure (Fig. 1) can store information related to the number of distinguishable configurations. For a cluster floating free in a medium, rotational symmetries can be trivially interchanged by global rigid rotations (and thus are not distinguishable), but mirror symmetries cannot. The number of distinguishable configurations for a cluster of  $N$  distinguishable spheres is  $N!/\sigma$ , where  $\sigma$  is the rotational symmetry of the cluster. In Fig. 1, an example  $N = 6$  cluster, which has an octahedral structure, is shown with six distinguishable outer spheres. The table in Fig. 1 provides the rotational symmetry and the maximum number of unique states for each spherical code structure up to  $N = 12$ . The  $N = 4$  cluster has two states that are mirror symmetries; this colloidal element can thus store a single bit. A cluster with  $s$  distinguishable states can store  $\log_2(s)$  bits of information or  $\log_2(s)/8$  bytes. As  $N$  increases, the amount of information storable in a cluster of size  $N$  increases as  $O(\ln(N!)) \approx O(N \ln(N))$ . A digital colloid with either 11 or 12 distinguishable spheres can therefore store 2.86 bytes in its spherical code structure.

In addition to the ability to store information, a digital colloid used for memory or computing must be able to switch – when appropriate – among the various distinguishable states accessible to it. We will consider each of these clusters of size  $N$  at values of  $\Lambda$  away from  $\Lambda_{SC}$ . However we will retain the constraint that each outer sphere must stay in contact with the inner sphere. An advantage of our particular implementation of a digital colloid is that the dynamics of the system can be excited or frozen by a small geometric change to the system. The dynamics exhibited by an  $N$ -cluster can be described in terms of three distinct regimes of  $\Lambda$ : forbidden, locked, and unlocked. If  $\Lambda < \Lambda_{SC}$ , the cluster is geometrically forbidden. If  $\Lambda_{SC} < \Lambda < \Lambda_T$ , the outer spheres are below their densest packing limit, and each sphere is caged by its neighbors and restricted to rattling about its spherical code coordinates. In this range each cluster



N	Point Group of Spherical Code	Rotational Symmetry	Storable States
4	$T_d$	12	2
5	$C_{4v}$	4	30
6	$O_h$	24	30
7	$C_{3v}$	3	1,680
8	$D_{4d}$	4	10,080
9	$D_{3h}$	18	20,160
10	$C_{2h}$	2	1,814,400
11	$C_{5v}$	5	7,983,360
12	$I_h$	60	7,983,360

Fig. 1 Left image: an  $N = 6$ , octahedral cluster. The outer spheres are transparent so the central particle can be seen. Middle image: the  $N = 6$  cluster labeled with six colors. On the right, a table shows the point group, rotational symmetry, and the maximum number of storable states for each  $N$ -cluster.

remains locked in an identifiable state given by its spherical code structure. If  $\lambda > \lambda_T$  the spheres are no longer caged and can rearrange to sample all of the states available to the cluster. The value of  $\lambda_T$  can be determined by geometrically constructing the cluster morphology of the transition state of a cluster.  $\lambda_T$  is thus the diameter ratio, above which the outer spheres may

permute so that transitions (T) among states may occur. We refer to a cluster in the regime  $\lambda > \lambda_T$  as “unlocked”. Fig. 2 shows the spherical code structure, point group symmetry, name of the convex polyhedron formed by the cluster (for those with names), and values of  $\lambda_{SC}$  and  $\lambda_T$  for each cluster in the range  $N = 4$ –12.

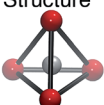
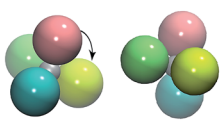

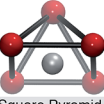
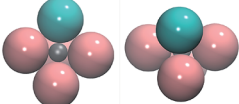
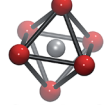
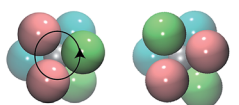
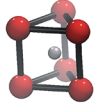
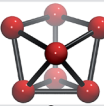
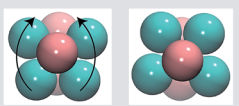
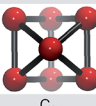
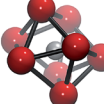
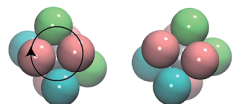
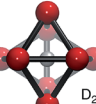
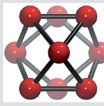
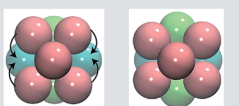
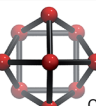
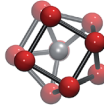
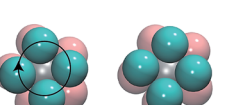
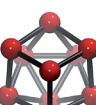

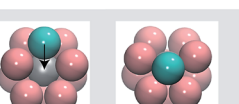
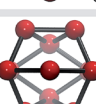
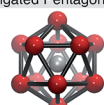
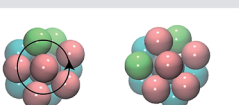
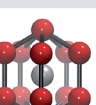

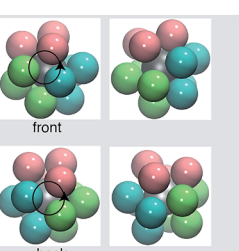

	Spherical Code Structure	$\lambda_{SC}$	Rearranging Move	Transition Structure	$\lambda_T$
N=4	 Tetrahedron, $T_d$	$\approx 0.2247$		 Square, $D_{4h}$	$\approx 0.4142$
N=5	 Square Pyramid, $C_{4v}$	$\approx 0.4142$		-	$\approx 0.4142$
N=6	 Octahedron, $O_h$	$\approx 0.4142$		 Triangular Prism, $D_{3h}$	$\approx 0.5275$
N=7	 $C_{3v}$	$\approx 0.5912$		 $C_{2v}$	$\approx 0.6005$
N=8	 Square Antiprism, $D_{4d}$	$\approx 0.6453$		 $D_{2d}$	$\approx 0.6676$
N=9	 $D_{3h}$	$\approx 0.7321$		 $C_{4v}$	$\approx 0.7418$
N=10	 $C_{2v}$	$\approx 0.8325$		 $C_{3v}$	$\approx 0.8340$
N=11	 Gyroelongated Pentagonal Pyramid, $C_{5v}$	$\approx 0.9021$		 $C_{2v}$	$\approx 0.9360$
N=12A	 Icosahedron, $I_h$	$\approx 0.9021$		 $D_{5h}$	= 1
N=12B	 Icosahedron, $I_h$	$\approx 0.9021$	 front back	 Anticuboctahedron, $D_{3h}$	= 1

Fig. 2 Left to right: the spherical code structure,  $\lambda_{SC}$ , unique rearrangement, transition structure, and  $\lambda_T$  for each cluster. The outer spheres in each rearrangement are colored so that the change in the cluster can be observed. The bonds (black) in the structures indicate spheres in contact.

When the central sphere is sufficiently large ( $\lambda \geq \lambda_T$ ), a finite set of cooperative rearrangements of outer spheres is permitted. The rearrangement pathways when  $\lambda \geq \lambda_T$  are unique to  $N$  and are reminiscent of the twisting of a Rubik's Cube™, the popular three-dimensional puzzle. Because each rearrangement follows a transition path between two identical spherical code structures, there is a midpoint on the path where the structure of the cluster is halfway between the two states. This transition state, which has mirror symmetry, is a saddle-point structure that the cluster must be able to form in order to rearrange. This transition state structure can be geometrically constructed, and the precise value of  $\lambda_T$  for any  $N$  may be numerically derived as the smallest  $\lambda$  for which the spheres can fit in the required shape. One exception to the transition pathway description is the  $N = 5$

cluster,<sup>26</sup> for which there is a continuum of structures, rather than a single, unique, transition structure (ESI-II†). The other exception is the  $N = 12$  cluster, which has two (possibly non-distinct) modes for rearranging its structure at  $\lambda_T$  (Fig. 2, ESI-movies†). When  $\lambda \gg \lambda_T$ , there is sufficient free surface that the dynamics of the outer spheres are uncorrelated.

An illustration of the cluster rearrangements and transition structures for every  $N$  is presented in Fig. 2. For the spherical code and transition structures, the black bonds represent spheres in contact. Although each cluster has a distinct transition path, the rotational symmetry of the cluster and chiral symmetry of the permutations imply there are multiple symmetrically equivalent ways the rearrangement can be excited in a given cluster. For example, there are five ways an  $N = 11$  cluster can rearrange. As shown in Fig. 4 (and ESI-I†), the rate of switching between states is sensitive to  $\lambda$ . Additional details regarding the calculations and the determination of accessibility of all states (ergodicity) can be found in Materials and methods. Movies of the rearrangements can be found in the online ESI.†

The predicted internal rearrangements of these digital clusters have two important consequences for information storage. First, every possible state can be reached by a sequence of rearrangements when  $\lambda > \lambda_T$ . This is demonstrated by showing that the group product of the rearrangement group and rotational symmetry group is equal to the symmetric group. Second, rearrangements can be switched on or off by toggling  $\lambda$  about  $\lambda_T$ . Consequently, a cluster's state may be erased by unlocking the cluster ( $\lambda > \lambda_T$ ), and a new state may be stored by locking it again ( $\lambda < \lambda_T$ ) after the cluster has rearranged.

All calculations so far have assumed an ideal system of perfectly hard outer spheres in perfect contact with an inner sphere. We have not studied in detail how much imperfection such a system can tolerate, for example, stretching of the

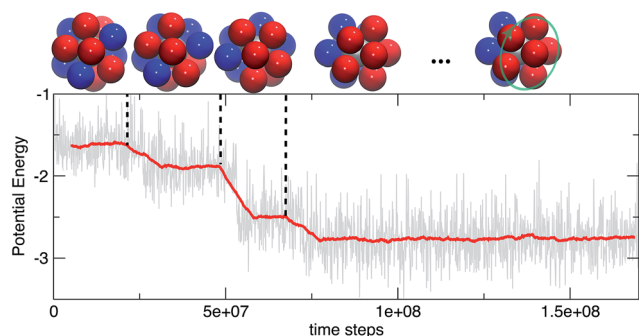


Fig. 3 The potential energy (grey) and averaged potential energy (red) of the rearrangements of an  $N = 12$  cluster as the cluster finds its lowest energy state. Snapshots of the interim states of the cluster are shown immediately above their position in the timeline. After time step  $7 \times 10^7$ , all rearrangements of the cluster correspond to the spherical cap of six red spheres rotating relative to the spherical cap of six blue spheres.

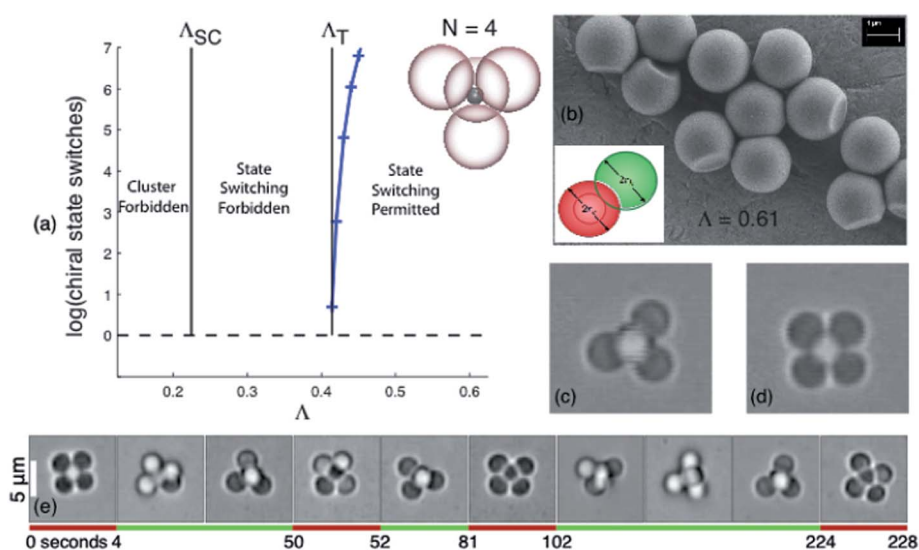


Fig. 4 (a) For  $N = 4$ , simulations predict state switching becomes measurable and increases rapidly for  $\lambda > \lambda_T$ . (b) An SEM micrograph of lock-and-key colloidal particles used to create the tetrahedral  $N = 4$  cluster shown in (c). (d) The cluster in its planar transition state. (e) A time series of micrographs showing typical reconfigurations of the cluster. Red bars indicate the planar transition state and green bars indicate tetrahedral order. Movies of the cluster dynamics and switching mechanism are in the ESI.†



inner-outer sphere bond or polydispersity. However, the simulations performed here and in ref. 26 modeled the spheres as slightly soft spheres. Additionally, ref. 26 also modeled the bonds as stretchable and breakable. This suggests that a reasonable amount of imperfection can be tolerated. For a digital colloid, however, the detachment of an outer sphere from the inner sphere would be considered a catastrophic event since the time required for an outer sphere to diffuse through the surrounding media and reattach to a transient gap appearing on the other side of the cluster is too long to be a dependable rearrangement mechanism. Also, if spheres can detach, then clusters cannot be locked.

If we consider the free energy landscape of a perfect sphere cluster for  $\lambda > \lambda_{SC}$ , the states should correspond to a set of low energy wells in the landscape connected by paths corresponding to transition states when  $\lambda > \lambda_T$ . (If  $\lambda$  is much greater than  $\lambda_T$ , the connecting paths will widen and the wells eventually disappear.) Conceptually, the addition of small irregularities in the particles should introduce minor perturbations to the position or depth of these wells, but not change their number. By introducing energy interactions between the spheres that drive the system to a given state, the number of wells should stay the same, but some wells will now be lower in depth than others. Energy interactions should be designed so that the cluster does not get kinetically trapped in a state that is not the lowest energy state. One advantage of all the wells being equally deep and all the transitions identical in the perfect system is that the design problem of accounting for small amounts of irregularity and successfully driving the system with energy interactions is a simplified. Since each state is symmetrically equivalent to every other state in the perfect system of equal state probabilities, if a set of energy interaction acts to kinetically funnel the system to a chosen state, then a symmetrically equivalent set of energy interactions can funnel the system to any other state.

These considerations also demonstrate why some clusters are better suited for information storage than others. As can be observed in the ESI† the depth of the energy wells associated with states of the ideal  $N = 10$  cluster is very small. Perturbing the energy landscape of this cluster with polydispersity and energy interactions would likely destroy the discrete nature of the states. However, the  $N = 4, 6$ , and  $12$  clusters have very deep energy wells around the states of their ideal clusters. We expect perturbing these clusters will not impact the gross features of the energy landscape. As a demonstration, in Fig. 3, we apply a simple set of energy interactions to a randomized simulated  $N = 12$  cluster. Beginning at  $t = 0$ , the blue spheres are attracted to the blue spheres and the red spheres are attracted to the red spheres. After three rearrangement, the  $N = 12$  cluster finds the low energy phase-separated state. Despite the perturbation to the system, the  $N = 12$  cluster is still found in a spherical code structure before and after each rearrangement.

The smallest cluster with at least two distinct states is the  $N = 4$  cluster. Our simulations predict the 4-cluster has tetrahedral symmetry, and so is capable of storing two states of opposite mirror symmetry when all four outer spheres are distinguishable from each other. We target a prototype tetramer

for experimental realization. In Fig. 4 we show an example of a 4-cluster assembled from  $1.8 \mu\text{m}$ -diameter colloidal particles dispersed in a density matched fluid medium. The particles are synthesized from monodisperse oil droplets *via* a free-radical polymerization. Each outer particle has a dimple formed by controlled buckling of the droplet's polymerized shell<sup>21</sup> whose curvature matches that of the central sphere. Four such dimpled particles can mate to each sphere, and are held in place by a depletion interaction<sup>20</sup> that yields thermodynamically stable clusters while still allowing the outer particles to move freely across the inner sphere's surface. Large quantities of these reconfigurable colloidal clusters self-assemble in highly concentrated suspensions. They are most easily visualized and analyzed, however, at low concentrations. The clusters used in this study therefore were assembled manually using holographic optical tweezers (Fig. 5).<sup>27,28</sup> Considerable effort was expended to ensure that the assembled clusters are neutrally buoyant so their behavior can be observed over periods extending to half an hour or more. Digital video images of the freely diffusing clusters were analyzed using specialized software<sup>29</sup> to track individually each of the particles in each of the clusters. Accounting for the dimple, the cluster in Fig. 3 has  $\lambda \cong 0.61$ . Based on our predicted value of  $\lambda_T = 0.4142$  (Fig. 2), this cluster should be unlocked and free to switch between states. To test this, we monitor the motion of the outer particles by recording their positions at a sufficiently high frame rate and tracking their relative positions within the cluster. We observe that the cluster is usually found in a tetrahedral structure like that shown in Fig. 4c. From time to time, however, it switches from one tetrahedral configuration to the equivalent structure with mirror symmetry. Further, we observe that this rearrangement occurs *via* the predicted planar transition structure (Fig. 4d), confirming the transition pathway anticipated in Fig. 2. These spontaneous rearrangements are shown in Fig. 6. To our knowledge, this is the first realization of a digital colloidal cluster. A description of the experimental procedure can be found in *Materials and methods* and short movies of the cluster dynamics and state switching can be found in the online ESI.†

The 4-cluster is the largest reconfigurable spherical code cluster we attempted to make. Although larger  $N$ -clusters can be

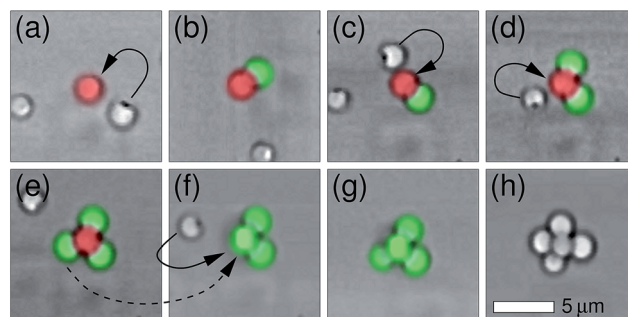


Fig. 5 Images of different steps during the assembly of a colloidal tetramer cluster using HOT. In (a–g), the inner sphere is red. The outer spheres, once attached are green. In (f and g), the inner sphere is visually obscured by an outer sphere.

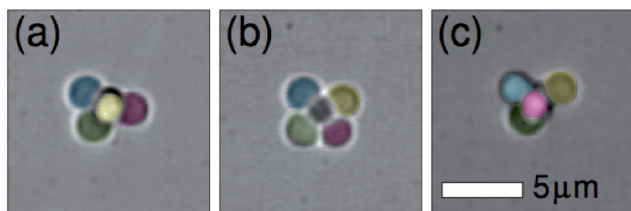


Fig. 6 Spontaneous reconfiguration of a colloidal tetramer. The outer spheres have been colored in the image to make the reconfiguration more apparent.

assembled using holographic optical tweezers, the serial nature of this technique precludes scaling to the large numbers of clusters desired for practical applications. Self-assembly offers an attractive alternative way to assemble large numbers of digital colloids of higher complexity. Simulations suggest that stable  $N$ -clusters will self-assemble from a bath of spheres if the outer spheres stick only to the inner spheres and if the diameter ratio  $\lambda$  of outer to inner spheres exceeds  $\lambda_{sc}$ .<sup>26</sup> Recent advances in colloidal synthesis and assembly suggest this should soon be possible. One particularly exciting route is the recent use of self-assembled colloidal crystals to template the fabrication of  $N = 12$  clusters, bringing the realization of 2.86 byte digital colloids within reach.<sup>30</sup> If issues of memory addressing could be solved, at just 3% concentration, a tablespoon of digital colloids in solution could store a terabyte of information.

In practice, digital colloids can store only as much information as can be written onto them and reliably read out. Writing to and reading from the digital colloids studied here are the next major challenges in utilizing them as wet computing elements. Experimentally, the first objective is to realize sufficient control over the cluster assembly process to create clusters readable by methods other than continuous imaging. A practical means of reading a cluster's configuration would be to use fluorescent microscopy. By labeling each halo particle with a unique fluorophore, a cluster's configuration could be determined from a single micrograph. Well-established image analysis techniques could be used to automate the process.<sup>29,31</sup> Reading larger clusters may require 3D imaging *via* confocal fluorescence, light sheet fluorescence, or the recently developed dual-view inverted selective plane illumination microscopy.<sup>32,33</sup> Image clarity can be enhanced to improve readout accuracy, by more closely matching the refractive index of particles and solvent. A wide variety of materials and solvents are available to achieve this,<sup>34</sup> once the fabrication of these digital colloids is more mature.

Reading, and then also writing, states may be achievable in ways other than imaging techniques. One example involves the use of Forster Resonant Energy Transfer (FRET). Particles functionalized with complementary FRET pairs would fluoresce when touching, allowing reading of the states of bulk quantities of  $N > 4$  clusters.<sup>35,36</sup> If an attractive or repulsive force can be induced between two spheres in the unlocked cluster (for  $N > 4$ , Fig. 7a), then the cluster will rearrange to adopt a state where the two spheres are or are not in contact, respectively. Such forces could be mediated by polymer brushes bound to the

colloid surfaces, a screened electrostatic potential, or the introduction of an amphiphile that binds to a specific sphere pair when they are in close proximity.

Additionally, by manufacturing the central particle from materials sensitive in volume to applied electric fields, changes in temperature, or changes in solvent composition,<sup>37–39</sup> we can permit or restrict structural transitions between stored states. Locking and unlocking the clusters' states could also be achieved by functionalizing the surface of the particles with complementary strands of DNA that would bind to one another with an appropriate change of temperature. This is a reversible process and could be used to freeze structural states to store information.<sup>40</sup>

The ability of reconfigurable colloidal clusters to store states and the sensitive control of the rate of switching between states suggests that such digital clusters may have a rich potential set of applications as small, information-storage elements. For

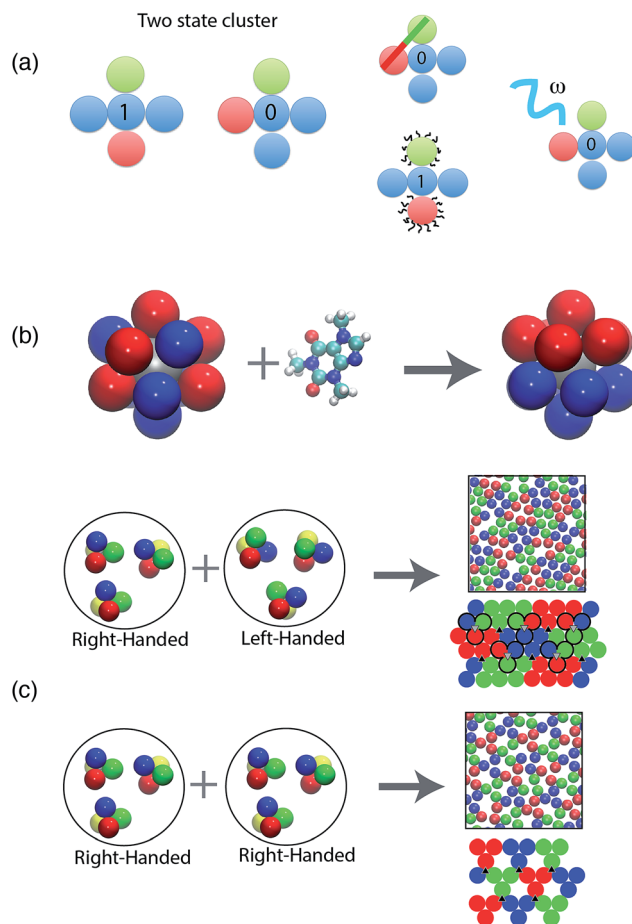


Fig. 7 (a) Schematic showing a cluster with two states determined by whether or not the red and green spheres are neighbors. Polymer brushes, block copolymers that bind to the spheres, and interactions with light may enable the states to be controlled and measured. (b) An  $N = 12$  cluster with two immiscible particle types reconfigures to a Janus cluster when it is exposed to a target chemical, swelling the central particle so as to unlock the cluster. (c) Two populations of 4-clusters are combined to self-assemble. Simulations predict two different resulting assemblies depending on whether the clusters have the same or opposite chirality.

example, a population of locked, identical  $N$ -clusters could be mixed into a controlled substance as a colloidal “bar code” that uniquely identifies the material’s origin. Digital colloids also could constitute a new class of sensors, devices capable of changing state in the presence of an external agent. Reconfigurable colloidal components could be designed to self-assemble into different mesoscale structures with measurable properties dependent on the clusters’ state. For example, a locked  $N = 12$  cluster, composed of two types of outer spheres randomly labeled, is shown in Fig. 7b. The interaction between the two types is designed to drive the spheres to de-mix when unlocked. When exposed to an environmental stimulus that unlocks the clusters, *e.g.* one that swells the central particle, our simulations predict the two outer sphere types separate and the cluster becomes a Janus particle.<sup>41</sup>

Another class of sensors could be created from a population of 4-clusters that are locked into a specific state and are designed to unlock when exposed to a certain environmental stimulus. When re-dispersed, an unlocked population of clusters would relax to a statistically uniform state that would signal the influence of the target stimulus. The difference could be observed macroscopically through the self-organization of the clusters, as illustrated in Fig. 7c.

Digital colloids also could act as a platform for localizing and controlling the transport of DNA-encoded information. Specific labels, for example, could be realized by grafting short oligonucleotides to the outer spheres prior to assembly.<sup>42–44</sup> Such hybrid DNA/nanoparticle components have already demonstrated potential in creating controllable assemblies. Although we describe here just a few envisioned uses of digital colloids, with targeted effort they could inspire a range of new nanoscale technologies based on soft matter, with real-world applications.

## Materials and methods

### Experimental clusters

Our practical realization of flexible colloidal clusters is created with colloidal lock-and-key particles<sup>20</sup> dispersed in a fluid medium. The central particle in each cluster is a colloidal sphere of radius  $r_c = 0.9 \mu\text{m}$ . Each outer particle is a colloidal sphere of the same nominal radius,  $r_h = 0.9 \mu\text{m}$  whose surface is marked by a single spherical dimple. Typical examples are shown in Fig. 3. An outer particle’s dimple can mate with the central sphere and can slide smoothly over the surface. Clusters of such spheres can be thermodynamically stabilized by depletion attractions mediated by dissolved polymers.<sup>20</sup> Tetrameric clusters, however, are unlikely to form spontaneously under typical experimental conditions because of substantial kinetic barriers to self organization.<sup>45</sup> We overcome these barriers by using holographic optical tweezers (HOT)<sup>27</sup> to assemble selected colloidal components into free-floating colloidal tetramers. Once assembled, the colloidal clusters are released, and their motions are followed by conventional methods of video microscopy.<sup>30</sup>

Our samples consist of a stoichiometric 4 : 1 mixture of dimpled spheres and spheres. The particles are synthesized from monodisperse oil droplets by free radical polymerization.

The oil consists of 3-methacryloxypropyl trimethoxysilane (TPM,  $\geq 98\%$ , Sigma-Aldrich) oligomers that are generated *in situ* through a base catalyzed condensation reaction between hydrolyzed TPM monomers.<sup>21</sup> Spherical particles are obtained using an oil-soluble initiator (2,2'-azo-bis-isobutyronitrile, AIBN, Sigma-Aldrich). Dimpled outer particles are polymerized with a water-soluble initiator (potassium persulfate, KPS, Sigma-Aldrich). The dimple is formed by controlled buckling of the droplets’ polymerized shells as described in ref. 21.

Filtered particles are redispersed in a density-matched solution of  $275 \text{ g L}^{-1}$  of sodium bromide (NaBr) in heavy water ( $\text{D}_2\text{O}$ ) at a nominal mass density of  $1.28 \text{ g mL}^{-1}$ . This high salt concentration screens the spheres’ Coulomb repulsion and leads to rapid irreversible aggregation. We therefore sterically stabilize the particles with Pluronic F-108 surfactant dissolved in the medium at 0.05 wt%. We also add  $0.01 \text{ g L}^{-1}$  of tetramethylammonium hydroxide (TMAH) to adjust the suspension’s pH to 9, thus maximizing the charge density on the particles’ surfaces.

Short-range depletion attractions are induced among the particles by dissolving polyethylene oxide (molecular weight 600 kDa, Sigma-Aldrich) in the fluid medium at a concentration of  $0.4 \text{ g L}^{-1}$ . This concentration is anticipated by the Asakura-Oosawa theory<sup>46</sup> to induce an inter-sphere contact attraction on the order of  $10 k_B T$  (ref. 20) where  $T = 298 \text{ K}$  is the absolute temperature. The attraction’s range is comparable to the polymers’ Gaussian-coil radius of 50 nm. The attraction between spheres and the close-fitting dimples of outer particles is expected to be several times stronger than this but with a comparable range.

Clusters are assembled and studied in a  $200 \mu\text{m}$  thick rectangular glass capillary tube (VitroCom) mounted on the stage of an inverted optical microscope (Nikon TE2000U). The capillary’s inner surfaces are roughened with a few covalently bound layers of 50 nm diameter silica nanoparticles (Polysciences, Inc., catalog #24040) to prevent depletion-induced particle deposition. The resulting surface roughness greatly weakens the particles’ attraction to the surface without severely degrading optical access. The sealed sample is observed with a  $100\times$  oil-immersion objective lens at a numerical aperture of 1.4 (Nikon Plan-Apochromat). This provides a system magnification of 135 nm per pixel when projected onto the sensor of a grayscale video camera (NEC TI 324A-II). The same objective lens also is used to project optical traps into the sample, which are used to manipulate individual colloidal particles into close enough proximity that they become flexibly bonded to each other by depletion attractions. The traps are powered by 0.9 W of laser light at a vacuum wavelength of 532 nm that is provided by a frequency-doubled solid-state laser (Coherent Verdi). The single laser is formed into multiple independently steered optical tweezers by a computer-designed hologram<sup>28</sup> that is imprinted on the light’s wavefronts with a liquid-crystal spatial light modulator (Holoeye Pluto).

Experimental movie 1† and Fig. 5 show the steps by which a colloidal tetramer is assembled with holographic optical tweezers. The central sphere initially is trapped and moved to the center of the microscope’s field of view. Additional traps are

used to localize dimpled spheres, which subsequently are moved to the central sphere's surface one at a time. Each outer particle is held in place until its dimple aligns with the central sphere's surface, at which point it sticks. Once the structure is complete, the optical tweezers are turned off and the colloidal tetramer is allowed to diffuse freely in the fluid medium.

As predicted by simulation, the colloidal cluster undergoes conformational transitions between two equivalent stable tetrahedral configurations. The transition passes through an unstable planar configuration in which the four outer particles are aligned on the corners of a square.

Experimental movie 2† shows a typical transition. The three images in Fig. 5 show the initial, transition, and final states in this process.

## Modeling methods

### Simulations

Using HOOMD-blue,<sup>47,48</sup> we performed Brownian dynamics simulations of pre-assembled clusters of outer spheres constrained to a central sphere surface. Outer sphere spheres interact *via* the WCA pair potential, shifted to a radius of  $3\sigma$  as per ref. 26. Each outer sphere has an effective diameter of  $d = 3.0786\sigma$ , as calculated per the Barker–Henderson eqn (2) in ref. 49. The outer spheres are restricted to the surface of the centrals, a constraint imposed during the integration of the equations of motion. This allows the dynamics of outer sphere rearrangement to be isolated from the dynamics of assembly and disassembly (the focus of ref. 26), and prevents any stretching of outer sphere–central bonds from influencing the structures observed. The central sphere diameter is defined as  $d_{\text{central}} = 2r_0 - d$ , where  $r_0$  is the fixed distance between the central and outer sphere centers. The central to outer sphere diameter ratio in the constrained system is thus  $\Lambda = d_{\text{central}}/d$  and varied by changing  $r_0$ .  $\Lambda$  is initialized such that the outer spheres can be sparsely randomly distributed on the surface (*i.e.*  $\Lambda \gg \Lambda_{\text{SC}}$ ), and then slowly decreased at the beginning of a simulation to a target  $\Lambda$ . The simulation is then run for  $10^9$  time steps while measuring properties and observing transitions.

### Characterizing the structure and transitions of the clusters

To characterize the structure, we measure the angular displacements between pairs of outer spheres. The angular displacement between two outer spheres bound to the same central sphere, or  $\theta = \angle H_1CH_2 \in [0, \pi]$ , is defined by the centers of two outer spheres  $H_1$  and  $H_2$  and the center of central sphere  $C$ . For a given  $N$  and  $\Lambda$ , the distribution of angular displacements  $n(\theta)$  reflects the structure of the cluster. Analogous to a pair correlation function,  $n(\theta)$  represents the likelihood of finding an outer sphere at an angular displacement  $\theta$  relative to the outer sphere, and  $\int n(\theta)d\theta = N - 1$ . To measure  $n(\theta)$  for a fixed  $N$  and  $\Lambda$ ,  $\angle H_1CH_2$  is measured over all outer sphere pairs every  $10^4$  time steps during a simulation with  $10^9$  total time steps.

For  $N = 4$ –12, Fig. SI-I-1† shows the  $n(\theta)$  of each  $N$ -cluster at three values of  $\Lambda$ :  $\Lambda_{\text{SC}}$  of the  $N$ -cluster, a middle value, and  $\Lambda_{\text{SC}}$

of the  $(N + 1)$ -cluster. The last represents the  $\Lambda$  where an additional outer sphere could be fit on the central surface. These three distributions are shown in order of increasing  $\Lambda$  from left to right.

For each  $N$ -cluster, in Fig. SI-I-1,† we observe a unique  $n(\theta)$  structure fingerprint that softens as  $\Lambda$  increases. For  $N > 4$ , each  $n(\theta)$  has multiple peaks. Except for  $N = 5$  and  $N = 10$ , at  $\Lambda = \Lambda_{\text{SC}}$  the first peak is narrow and not connected to other peaks, indicating outer spheres are locally caged at their spherical code points. The width of a peak is proportional to the rattling of an outer sphere within its local cage. As  $\Lambda$  increases, the peaks broaden and eventually become connected. This broadening and overlapping is associated with the degradation of the well-defined structure by increased rattling and sporadic rearranging. In no case did we find any evidence of new stable structures emerging. For the clusters  $N = 5$  and  $N = 10$  the peaks are connected at even the smallest  $\Lambda$  considered. For these two clusters,  $\Lambda_{\text{T}} - \Lambda_{\text{SC}}$  is zero or almost zero and the free energy barrier to rearranging is very small.

For all  $N$ , if  $\Lambda \gg \Lambda_{\text{T}}$ , then the outer spheres sample uniformly random arrangements on the central surface and the  $n(\theta)$  distribution is a cosine function of  $\theta$ , truncated to zero when  $\theta$  is less than the angular diameter of a single outer sphere. Insofar as the distributions are far from cosine functions, and thus the outer spheres are far from randomly distributed on surface, the  $N$  clusters adopt structures derived from their underlying spherical code solution over the entire range of  $\Lambda$  considered.

To measure the transitions of the clusters, we find quantities that measurably change over a transition. For the  $N = 4$  cluster, while the chirality of the cluster can switch, all outer spheres are always neighbors with all other outer spheres, so the angular displacement between two outer spheres does not discretely change. So, chirality switches are measured as follows. The cluster is arbitrarily divided into two outer sphere pairs ( $A, B$ ), and ( $C, D$ ). Let the vector from the center of the central to the center of each outer sphere be labeled as  $\vec{A}$ ,  $\vec{B}$ ,  $\vec{C}$ , and  $\vec{D}$  respectively. The following is calculated.

$$f = \text{sign}(((\vec{A} \times \vec{B}) \times (\vec{C} \times \vec{D})) \cdot (\vec{A} + \vec{B}))$$

When  $f$  changes from  $-1$  to  $1$  or  $1$  to  $-1$ , this indicates the cluster has flipped chirality.

In Fig. SI-I-2,† the logarithm of the number of times a cluster flips over  $10^9$  time steps is shown as a function of  $\Lambda$ .

For  $N > 4$ , if a cluster is able to rearrange its outer spheres, two outer spheres that are neighbors will eventually not be neighbors (and *vice versa*), that is, the angle  $\theta$  between them will change by a discrete jump. So to measure transitions in a cluster structure, we can measure the decorrelation of the angular displacements. To characterize the dynamics of a cluster, we calculate the time scale over which  $\theta$  is no longer correlated with itself. We define the state switching parameter  $\tau$  from

$$C(\theta(t), \theta(t + \delta t)) = e^{-t/\tau}$$



where  $C(\theta(t), \theta(t + \delta t))$  is the normalized angular autocorrelation function and  $t$  is time. In this work,  $\tau$  has units of  $1/10\,000$  time steps. The more mobile an outer sphere is on the surface of the central, the more rapidly its angular displacement decorrelates. When the rate of decay of angular correlations is zero, all the outer spheres in the cluster are fully caged. We only calculate  $\tau$  for clusters that display more than one distinct peak in their  $n(\theta)$  distributions (*i.e.*  $N > 4$ ) so that position swapping can be distinguished from local rattling. The lower bound on the  $\tau$  measurement is  $1.5 \times 10^{-4}$ ; below this the outer sphere positions swaps occur too infrequently over a  $10^9$  time step simulation for accurate values of  $\tau$  to be measured. We calculate  $\tau$  as a function of  $N$  and  $\Lambda$ . In Fig. SI-I-3,† for each  $N$ -cluster, we plot the state switching parameter as a function of  $\Lambda$ . In each figure, as  $\Lambda$  increases, the rate of angular decorrelation also increases.

The parameters  $\Lambda_{SC}$  and  $\Lambda_T$  are calculated from geometric considerations of perfectly hard spheres. Because the outer spheres in the simulation are not perfectly hard, it is possible for meaningful measurements to be made when  $\Lambda < \Lambda_{SC}$  and for the outer spheres to rearrange at  $\Lambda < \Lambda_T$  for an energy cost of overlapping slightly. We observe, in general, the larger the gap between  $\Lambda_{SC}$  and  $\Lambda_T$ , the larger the gap between  $\Lambda_T$  and the  $\Lambda$  where the soft spheres outer spheres are first measured to rearrange. This indicates the larger the difference between the spherical code structure and the transition structure, the greater the free energy barrier to form the transition structure.

### Calculation of $\Lambda_T$

To determine the transition structure of each  $N$ -cluster, we first use simulation to observe the approximate transition structure that appears during a transition event. This transition structure generally has a high symmetry and can be described by a network of contacts between the outer spheres. We then geometrically determined the smallest value of  $\Lambda$  that, in the mathematical limit of hard spheres, could form a structure of that symmetry and contact network. This geometrically constructed structure with perfectly hard spheres determines  $\Lambda_T$ . The only assumption we make is that the mathematically exact transition structure at  $\Lambda = \Lambda_T$  will have the same morphology as can be observed in an approximate transition structure at  $\Lambda > \Lambda_T$ . Provided a transition event is still a rare but observable event in the simulation, the value of  $\Lambda_T$  constructed geometrically should have no sensitivity to the details of the simulation used to derive it.

For each cluster,  $N = 4$ –12, there is a value of  $\Lambda$  where the angles between outer spheres is first observed to decorrelate over a simulation of length over a  $10^9$  time steps. At this value of  $\Lambda$ , the dynamics of the cluster during a transition were observed for many transitions. A minimum of ten rearranging moves were observed, and for  $N = 4$ –11, confirmed to be identical (barring a rotation or mirror symmetry operation). For  $N = 12$  two rearranging moves were found (12A, 12B). Each rearranging move, observed as a sequence of snapshots issued one per time step, of the outer sphere coordinates, was found to be time symmetrical from the beginning to the ending spherical code structure. At the middle of the sequence is found a snapshot

where the cluster has a structure with mirror symmetry that is halfway between the beginning and ending spherical code structure. From this snapshot, we observe the symmetry of the structure and the contact network of the outer spheres. This information was then used to geometrically construct the densest arrangement of points on the surface of a sphere that satisfies both.

For the case of  $N = 4, 6, 7, 8, 9, 10$ , and  $12B$ , only one structure can be constructed that satisfies symmetry and contact network. For  $N = 11$ , ten of the outer spheres shift slightly to permit the eleventh outer sphere to jump from its spherical code coordinate to the vacancy. A series of iterative steps that preserved the symmetry of the cluster while compressing the 11 outer spheres was used to find the optimal densest arrangement.

For  $N = 7, 8, 9$ , and  $12A$ , the structure formed has the symmetry of, and is closely related to, the Johnson solids, J49 (Augmented Triangular Prism), J84 (Snub Disphenoid), J10 (Gyroelongated square pyramid), and J16 (elongated pentagonal bipyramid), respectively. However, the vertices of these Johnson solids are not found on the surface of a single sphere, so the transition structure is a distorted version of these polyhedra.

For the rearranging move  $N = 12A$ , we observe that the transition structure shown in Fig. 2 of the main text with symmetry  $D_{5h}$  may only be the approximate transition structure. We note that the middle spheres of 5 half-great circles in the  $N = 12A$  transition have only two neighbor contacts in the longitudinal direction and thus are under constrained. The distance between neighboring particles in the rotating ring is only 1.8% larger the distance between contacting particles. It is possible that this cluster has a slightly smaller  $\Lambda_T$  and that the ring rotation actually occurs by a sequence of spheres sliding past each other, and thus, there is a sequence of transition states, reminiscent of how, for example, a supramolecular helix changes handedness.<sup>50</sup> However, this sequence of moves likely occurs at such a small deviation in  $\Lambda$  from the full ring rotation that we did not measure any impact on the state switching of the cluster.

For each cluster, one can postulate other types of transitions with other associated transition structures. For the small  $N$  clusters studied here there is apparently a gap in  $\Lambda$  between the lowest excitable transition and the next excitable transition. In some or all cases, that gap may well be large enough that the next excitable transition is never observable.

### Ergodicity

Consider the  $N$ -th spherical code as having  $N$  lattice positions 1, 2, 3, ...  $N$  and the spheres on the lattice having identities  $A, B, C, \dots$ . In a single snapshot of the system, each sphere is assigned to a lattice point (*e.g.* 1:  $A$ , 2:  $B$ , 3:  $C$ , ...). The set of possible ways to permute the assignment of the spheres to lattice points form a permutation group. For a finite set of  $N$  elements, the symmetric group of the set is the set of all permutations of the set, which has  $N!$  members. Each permutation group is a subgroup of the symmetric group. If the cluster is not mobile, *i.e.* all outer sphere are locally caged, then the permutation group of the

cluster is the rotational symmetry group of the cluster. When the cluster is mobile, there are additional group generators that permute the cluster. For  $N = 4$ –12 we calculated that the permutation group generated when the cluster is first observed to rearrange is equal to the symmetric group. We identified the generators of the permutation group using disjoint cyclic notation, and then use the software of ref. 51 to generate the whole group. For each case we found that the group generated is the same size as the symmetric group, and thus is the symmetric group.

Thus we show that the mobile  $N = 4$ –12 clusters are ergodic. That is, over time, every possible configuration of spheres is generated. There is no arrangement that cannot be reached by the rearranging actions alone. All states (permutations) have the same free energy and are equally likely. The only exception to this finding is the rearrangement 12A, which has an orbit that does not include the entire state space. However, the rearrangement 12B, which is also excited at  $A_T = 1$ , does make every state accessible.

For comparison, this property is not true for the corner and edge cubes of a Rubik's cube. There are configurations of a Rubik's cube that can only be generated by illegally disassembling and reassembling the cube.

### Simulation details for the assembly of an $N = 12$ Janus cluster

Using HOOMD-blue,<sup>47,48</sup> we performed a Brownian dynamics simulation of an  $N = 12$  cluster with  $A = 1.06$ . The outer spheres have two species,  $H_1$ , and  $H_2$ . Initially all the spheres interact *via* a Weeks–Chandler–Anderson (WCA) pair potential ( $\epsilon = 1.0$ ,  $\sigma = 1.0$ ,  $r_{\text{cut}} = 2^{1/6}$ ). After initializing and equilibrating the cluster, an attraction is turned on between like spheres *via* a shifted Lennard Jones potential ( $\epsilon = 0.2$ ,  $\sigma = 1.0$ ,  $r_{\text{cut}} = 2.5$ ). In three rearrangements, shown in Fig. SI-III-1,† the  $N = 12$  cluster has found the phase separated “Janus” configuration. All subsequent rearrangements observed correspond to rotating the red cap relative to the blue cap. A simulation performed with  $A = 1.0$  was not observed to rearrange over  $1 \times 10^9$  time steps.

### Simulation details for assembly of $N = 4$ clusters into lattices

Using HOOMD-blue,<sup>47,48</sup> we performed Brownian dynamics simulations of a system of clusters of mixed chirality and a system of clusters of a single chirality interacting while bound to a plane. Clusters were modeled as three spheres, of identity  $A$ – $B$ – $C$  or  $A$ – $C$ – $B$ , rigidly connected in a triangle and able to move freely in a plane. This models a system of tetramers where a fourth particles “ $D$ ”, is attracted to a surface. Unlike spheres interacted *via* a WCA pair potential ( $\epsilon = 1.0$ ,  $\sigma = 1.0$ ,  $r_{\text{cut}} = 2^{1/6}$ ). Like spheres interacted *via* a shifted Lennard Jones potential ( $\epsilon = 1.0$ ,  $\sigma = 1.0$ ,  $r_{\text{cut}} = 2.5$ ). Two simulations were run, one with 400 same chirality clusters ( $A$ – $B$ – $C$ ), and one with 200 clusters of each chirality ( $A$ – $B$ – $C$  and  $A$ – $C$ – $B$ ). The system was simulated at a number density of  $0.16/\sigma^2$  and cooled from a high temperature to a temperature where self-assembly of a regular structure was observed, over  $10^6$  time steps. Over the annealing the clusters transform from a disordered random state, condense into a droplet, and organize into a regular structure.

We observe the system with clusters of all the same chirality forms an open lattice structure with a  $\sim 68\%$  packing density. We observe the system with clusters of mixed chirality forms a dense hexagonal structure with a  $\sim 91\%$  packing density. The two structures are depicted diagrammatically in Fig. 7c. We did not verify that either ordered structure is a unique ground state for the system.

## Acknowledgements

The work of S.C.G., D.J.P., K.V.E. B.J.K. and S.S. to design and conduct the experiments were supported by the U. S. Army Research Office under MURI Grant Award no. W911NF-10-1-0518. Conception of the idea and the initial theoretical and computational work by C.L.P., E.J. and S.C.G. was supported by the Biomolecular Materials Program, U. S. Department of Energy Office of Science, under award DE-FG02-02ER46000. SCG also acknowledges the Simons Investigator program of the Simons Foundation. C.L.P. was funded by the Office of the Director through the Named Postdoctoral Fellowship Program (Aneesur Rahman Postdoctoral Fellowship), Argonne National Laboratory. Use of the optical tweezers (B.J.K. and D.G.G.) was supported by the MRSEC program of the National Science Foundation through Grant number DMR-0820341.

## References

- 1 L. Adleman, Molecular computation of solutions to combinatorial problems, *Science*, 1994, **266**, 1021–1024.
- 2 R. J. Lipton, DNA solution of hard computational problems, *Science*, 1995, **268**, 542–545.
- 3 P. W. K. Rothmund, Folding DNA to create nanoscale shapes and patterns, *Nature*, 2006, **440**, 297–302.
- 4 L. Qian and E. Winfree, Scaling Up Digital Circuit Computation with DNA Strand Displacement Cascades, *Science*, 2011, **332**, 1196–1201.
- 5 Y. Amir, E. Ben-Ishay, D. Levner, S. Ittah, A. Abu-Horowitz and I. Bachlet, Universal computing by DNA origami robots in a living animal, *Nat. Nanotechnol.*, 2014, **9**, 353–357.
- 6 A. Adamatzky, B. D. L. Costello and T. Asai, *Reaction-Diffusion Computer*, Elsevier, 2005.
- 7 M. Prakash and N. Gershenfeld, Microfluidic Bubble Logic, *Science*, 2007, **315**, 832–835.
- 8 S. Kou, *et al.*, Fluorescent Molecular Logic Gates Using Microfluidic Devices, *Angew. Chem., Int. Ed.*, 2008, **47**, 872–876.
- 9 G. M. Church, Y. Gao and S. Kosuri, Next-Generation Digital Information Storage in DNA, *Science*, 2012, **337**, 1628.
- 10 F. Ilievski, *et al.*, Soft Robotics for Chemists, *Angew. Chem., Int. Ed.*, 2011, **50**, 1890–1895.
- 11 K. Sun, T. S. Wei, B. Y. Ahn, J. Y. Seo, S. J. Dillon and J. A. Lewis, 3D Printing of Interdigitated Li-Ion Microbattery Architectures, *Adv. Mater.*, 2013, **25**, 4539–4543.
- 12 J. J. Adams, *et al.*, Conformal Printing of Electrically Small Antennas on Three-Dimensional Surfaces, *Adv. Mater.*, 2011, **23**, 1335–1340.

- 13 W. Wu, A. J. DeConinck and J. A. Lewis, Omnidirectional Printing of 3D Microvascular Networks, *Adv. Mater.*, 2011, **23**(178–183).
- 14 C. Papadimitriou, Computational complexity, *Ency. of Comp. Sci.*, 2003, pp. 260–265.
- 15 H. Abelson, *et al.*, Amorphous computing, *Commun. ACM*, 2000, **43**, 74–82.
- 16 D. Servat and A. Drogoul, Combining amorphous computing and reactive agent-based systems: a paradigm for pervasive intelligence?, *AAMAS '02 Proc. of the first inter. joint conf. on Autonomous agents and multiagent systems: part 1*, 2002, pp. 441–448.
- 17 S. C. Glotzer and M. J. Solomon, Anisotropy of building blocks and their assembly into complex structures, *Nat. Mater.*, 2007, **6**, 557–562.
- 18 S. Mann, Self-assembly and transformation of hybrid nano-objects and nanostructures under equilibrium and non-equilibrium conditions, *Nat. Mater.*, 2009, **8**, 781–792.
- 19 M. J. Solomon, Materials science: Reconfigurable colloids, *Nature*, 2010, **464**, 496–498.
- 20 S. Sacanna, W. T. M. Irvine, P. M. Chaikin and D. J. Pine, Lock and Key Colloids, *Nature*, 2010, **464**, 575–578.
- 21 S. Sacanna, W. T. M. Irvine, L. Rossi and D. J. Pine, Lock and key colloids through polymerization-induced buckling of monodisperse silicon oil droplets, *Soft Matter*, 2011, **7**, 1631–1634.
- 22 F. Toth, *Regular Figures*, The Macmillan Company, 1964.
- 23 T. W. Melnyk, O. Knop and W. R. Smith, Extremal arrangements of points and unit changes on a sphere: equilibrium configurations revisited, *Can. J. Chem.*, 1977, **55**, 1745–1761.
- 24 L. L. Whyte, *Unique arrangement of points on a sphere*, The American Mathematical Monthly, vol. 59, 1952, pp. 606–611.
- 25 N. J. A. Sloane, with the collaboration of R. H. Hardin, W. D. Smith and others, Tables of Spherical Codes, Coverings, Maximum Volume of Convex Hulls, and Minimal Energy Arrangements published electronically at <http://www.research.att.com/~njas/>.
- 26 C. L. Phillips, E. Jankowski, M. Marval and S. C. Glotzer, Self-assembled clusters of spheres related to spherical codes, *Phys. Rev. E: Stat., Nonlinear, Soft Matter Phys.*, 2012, **86**, 041124.
- 27 D. G. Grier, A revolution in optical manipulation, *Nature*, 2003, **424**, 810–816.
- 28 M. Polin, K. Ladavac, S.-H. Lee, Y. Roichman and D. G. Grier, Manipulation and assembly of nanowires with holographic optical traps, *Opt. Express*, 2005, **13**, 5831–5845.
- 29 J. C. Crocker and D. G. Grier, Methods of Digital Video Microscopy for Colloidal Studies, *J. Colloid Interface Sci.*, 1996, **179**, 298–310.
- 30 J. T. McGinley, I. Jenkins, T. Sinno and J. C. Crocker, Assembling colloidal clusters using crystalline templates and reprogrammable DNA interactions, *Soft Matter*, 2013, **9**, 9119–9128.
- 31 G. L. Hunter, K. V. Edmond, M. T. Elsesser and E. R. Weeks, Tracking rotational diffusion of colloidal clusters, *Opt. Express*, 2011, **19**, 17189.
- 32 A. D. Dinsmore, E. R. Weeks, V. Prasad, A. C. Levitt and D. A. Weitz, Three-dimensional confocal microscopy of colloids, *Appl. Opt.*, 2001, **40**, 4152–4159.
- 33 Y. Wu, P. Wawrzusin, J. Senseney, R. S. Fischer, R. Christensen, A. Santella, A. G. York, P. W. Winter, C. M. Waterman, Z. Bao, D. A. Colon-Ramos, M. McAuliffe and H. Shroff, Spatially isotropic four-dimensional imaging with dual-view plane illumination microscopy, *Nat. Biotechnol.*, 2013, **31**, 1032.
- 34 S. Wiederseiner, N. Andreini, G. Epely-Chauvin and C. Ancey, Refractive-index and density matching in concentrated particle suspensions: a review, *Exp. Fluids*, 2011, **50**, 1183.
- 35 L. Cerdán, E. Enciso, V. Martín, J. Bañuelos, I. López-Arbeloa, A. Costela and I. García-Moreno, FRET-assisted laser emission in colloidal suspensions of dye-doped latex nanoparticles, *Nat. Photonics*, 2012, **6**, 621–626.
- 36 L. Wang and W. Tan, Multicolor FRET Silica Nanoparticles by Single Wavelength Excitation, *Nano Lett.*, 2006, **6**, 84–88.
- 37 T. Still, K. Chen, A. M. Alsayed, K. B. Aptowicz and A. G. Yodh, Synthesis of micrometer-size poly(N-isopropylacrylamide) microgel particles with homogeneous crosslinker density and diameter control, *J. Colloid Interface Sci.*, 2013, **405**, 96.
- 38 K. Kratz, T. Hellweg and W. Eimer, Influence of charge density on the swelling of colloidal poly-(N-isopropylacrylamide-co-acrylic acid) microgels, *Colloids Surf., A*, 2000, **170**, 137–149.
- 39 L. Farias-Cepeda, J. Herrera-Ordóñez and E. Saldívar-Guerra, Effect of surfactant on the swelling of polymeric nanoparticles: toward a generalized approach, *Colloid Polym. Sci.*, 2009, **287**, 1215–1220.
- 40 N. Geerts and E. Eiser, DNA-functionalized colloids: Physical properties and applications, *Soft Matter*, 2010, **6**, 4647.
- 41 P.-G. de Gennes, Soft Matter (Nobel Lecture), *Angew. Chem., Int. Ed.*, 1992, **31**, 842–845.
- 42 P. L. Biancaniello, A. J. Kim and J. C. Crocker, Colloidal interactions and self-assembly using DNA hybridization, *Phys. Rev. Lett.*, 2005, **94**, 058302.
- 43 M.-P. Valignat, O. Theodoly, J. C. Crocker, W. B. Russel and P. M. Chaikin, Reversible self-assembly and directed assembly of DNA-linked micrometer-sized colloids, *Proc. Natl. Acad. Sci. U. S. A.*, 2005, **102**, 4225.
- 44 D. Nykypanchuk, M. M. Maye, D. van der Lelie and O. Gang, DNA-guided crystallization of colloidal nanoparticles, *Nature*, 2008, **451**, 549–552.
- 45 J. C. Crocker, J. A. Matteo, A. D. Dinsmore and A. G. Yodh, *Phys. Rev. Lett.*, 1999, **82**, 4352–4355.
- 46 S. Asakura and F. Oosawa, *J. Chem. Phys.*, 1954, **22**, 1255–1256.
- 47 *HOOMD-blue*, 2010, <http://codeblue.umich.edu/hoomd-blue/>.

- 48 C. L. Phillips, J. A. Anderson and S. C. Glotzer, *J. Comp. Physiol.*, 2011, **230**, 7191–7201.
- 49 J. A. Barker and D. Henderson, *J. Chem. Phys.*, 1967, **47**, 4714.
- 50 D. Chakrabarti and D. J. Wales, *Soft Matter*, 2011, **7**, 2325.
- 51 *GAP, Groups, Algorithms, and Programming, Version 4.4.12*, The GAP Group(2008).